Effect of Reynolds number on TiO_2 nanosponges doped with Li^+ cations

Blasco-Tamarit, E.; Muñoz-Portero, M.J.; Sánchez-Tovar, R.; Fernández-Domene, R.M.; García-Antón, J.*

Ingeniería Electroquímica y Corrosión (IEC). Departamento de Ingeniería Química y Nuclear. ETSI Industriales. Universitat Politècnica de València. Camino de Vera s/n, 46022 Valencia, Spain.

Tel. 34-96-387 76 32, Fax. 34-96-387 76 39, e-mail: jgarciaa@iqn.upv.es

Abstract

Anatase TiO_2 nanosponges have been synthesized by anodization of Ti, and Li^+ cations have been inserted in these nanostructures. The influence of hydrodynamic conditions (Reynolds number, Re = 0 to Re = 600) during anodization has been studied. Li-doped TiO_2 nanosponges were characterized by Field Emission Scanning Electron Microscopy (FE-SEM), Raman confocal microscopy, Electrochemical Impedance Spectroscopy (EIS) and Mott-Schottky analysis (M-S). Photoelectrochemical performance and resistance to photocorrosion measurements were also carried out. Li-TiO_2 nanosponges proved to be better photocatalysts for water splitting than Li-TiO_2 nanotubes. Moreover, the photoelectrochemical behavior of the Li-doped nanosponges improved as Reynolds number increased.

Keywords: Anatase TiO_2; nanostructured materials; Li^+ intercalation; photoelectrocatalyst; anodization.

1. Introduction

TiO_2 is one of the most widely studied compounds in materials science. Owing to some outstanding properties it is used in dye-sensitized solar cells, biomedicine, electrochromic and self-cleaning devices, gas sensors and photocatalytic reactions [1–11]. Especially, TiO_2 is used as a photocatalyst due to its high stability and semiconductor abilities that are able of generating charge by absorbing energy [12–15]. Besides, its suitable band-edge positions allow the photoelectrochemical water splitting [16] into H_2 and O_2 using solar energy. This H_2 is a potential fuel of the future.

Many TiO_2 applications require to maximize its specific surface area to achieve a maximum efficiency. Thus, TiO_2 has been synthesized into different nanostructures such as nanoparticles [17–19], nanorods/nanowires [19–21] or nanotubes [17,18,22-34]. These nanostructures are synthesized by several methods, including sol-gel transcription [36,37] or hydrothermal processes [38,39]. Anodization of titanium in fluoride-based electrolytes is other possible method, in fact it is one of the most promising method to synthesize TiO_2 nanotubes because it allows obtaining highly ordered nanotube arrays directly grown into the Ti substrate, and their dimensions (length, diameter, and tube wall) can be precisely controlled [40–42]. In previous works, the authors showed that under specific anodization in glycerol/water electrolytes and using hydrodynamic conditions, a transition from a TiO_2 nanotube morphology (stagnant conditions) to a nanosponge morphology (hydrodynamic conditions) occurs [34,43,44]. These nanosponges provide better performance for water splitting than the tube morphologies obtained in glycerol/water electrolytes [34].

The nanostructures formed after electrochemical anodization are amorphous, which implies the presence of a high number of defects that act as recombination centers and diminish their efficiency as photocatalysts. In general, these amorphous nanostructures can be converted into crystalline ones using a thermal treatment in air: anatase (300-500 °C) or rutile (> 500 ºC) [45–47]. After conversion to anatase, the bandgap results in 3.2 eV and in 3.0 eV if annealing is performed to form rutile [26,48]. In spite of the narrower bandgap of rutile, annealing treatments that lead to a complete conversion to rutile have not been successfully carried out because the nanostructure tends to undergo significant morphological deterioration (sintering and collapse) at around 700 ºC [46,47]. However, anatase structure has a significantly higher charge carrier mobility than rutile, which is very important in photoelectrochemical applications, and it is a suitable material to decompose water into hydrogen and oxygen under illumination [46,47].

The intrinsic bandgap of anatase (3.2 eV) allows the material to absorb light only in the UV range, which means that only about 5-7% of the solar spectrum can be absorbed [49]. One of the methods to extend the solar spectrum to the visible range is the insertion of doping elements in the nanostructure. In fact, another special feature of TiO_2 is the ability to insert small ions into its lattice, which increases its donor density or/and its conductivity [50,51]. The insertion of these ions into the TiO_2 nanostructures allows modulating their electrical properties and narrowing the bandgap, thus, increasing the efficiency of TiO_2 nanostructures. Several authors [45,46,52,53] studied the insertion of Li^+ cation into the TiO_2 lattice and reported a drastic change in its electronic properties, such as a higher TiO_2 conductivity [52,53]. However, these studies were made for TiO_2 nanotubes, and a complete study on Li-doped TiO_2 nanosponges

synthesized in glycerol/water electrolytes under hydrodynamic conditions has not been evaluated yet.

In this work, Li-doped nanosponges of anatase TiO_2 obtained by anodization of Ti in glycerol/water/NH_4F electrolytes have been synthesized to be used as photocatalysts in photoelectrochemical water splitting for hydrogen production using sunlight. The influence of hydrodynamic conditions during anodization has been studied to increase efficiency. To characterize the nanostructures, different microscopy techniques have been used: Field Emission Scanning Electron Microscope (FE-SEM) and Raman confocal microscopy. Electrochemical measurements (Electrochemical Impedance Spectroscopy (EIS) and Mott-Schottky analysis (M-S)), as well as photoelectrochemical techniques, have also been used.

2. Experimental procedure

Anodization under hydrodynamic conditions was performed in a two electrodes electrochemical cell with a rotating electrode configuration. A Teflon-coated Grade 2 titanium rod (8 mm in diameter) was used as a working electrode with 0.5 cm^2 of surface exposed to the electrolyte, and a platinum foil was used as a counter electrode. Both electrodes were connected to a voltage source. The titanium rods were mounted in a rotating electrode to perform the anodization under hydrodynamic conditions (**Figure 1**).

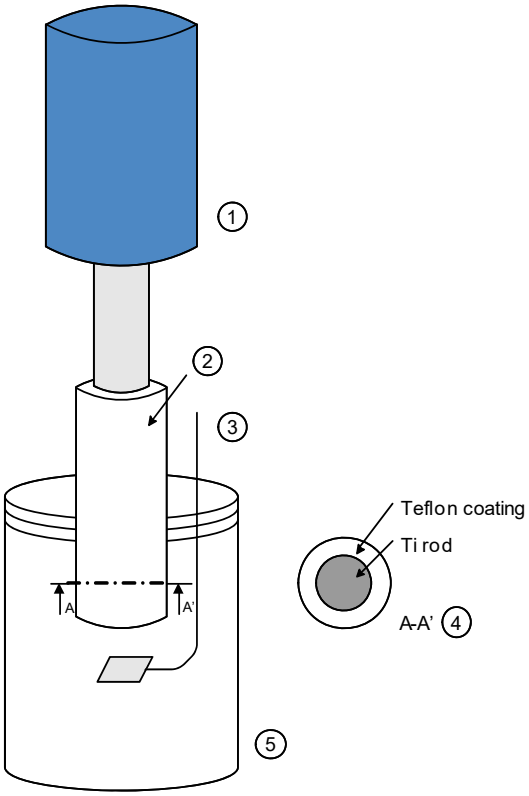

Figure 1. Scheme of the electrochemical cell with the RDE used in the anodization tests: (1) RDE, (2) Ti electrode, (3) platinum counter electrode, (4) cross-section of the Ti electrode showing the Teflon coating, (5) electrochemical cell.

Prior to anodization, the titanium surface was abraded with 220 to 4000 silicon carbide (SiC) papers and degreased by sonication in ethanol for 2 minutes. Different Reynolds numbers (Re) were used: 0, 200, 400 and 600, which correspond to 0, 1307, 2614 and 3921 rpm. The Reynolds numbers were calculated as follows:

$$\mathrm{Re} = \frac{\omega \cdot r^2 \cdot \rho}{\mu} \qquad \textbf{(1)}$$

where ω is the rotation speed expressed in rad s^{-1}, r is the radius of the working electrode in cm and ρ and μ are the density in g cm^{-3} and the dynamic viscosity in g cm^{-1} s^{-1} of the solution, respectively [43].

Anodization was performed in a mixture of glycerol/ water (60:40 vol.%) with a concentration of 0.27 M of NH_4F. The anodization volume was 30 mL. The samples were anodized at 30 V for three hours. Current density during anodization was measured versus time.

After anodization, the titanium rod was cut to carry out different tests. The morphology of the obtained nanostructures was characterized by using Field Emission Scanning Electron Microscopy (FE-SEM). The anodized samples were annealed at 450 ºC in air for 1 hour (heating at 30 $ºC \cdot s^{-1}$) in order to transform amorphous TiO_2 to an anatase phase structure. The crystalline microstructure of TiO_2 was examined by means of a Raman Confocal Laser microscope using a 632 nm neon laser with 420 μW.

In order to dope the nanostructures with Li^+, the samples were immersed in a 1M $LiClO_4$ solution and a potential of -1.5 $V_{Ag/AgCl}$ was applied for 3 seconds. In this way, Ti^{+4} was reduced to Ti^{+3} and, at the same time, Li^+ was inserted into the TiO_2 lattice. This Li^+ insertion was performed in a three electrode electrochemical cell, using the annealed-TiO_2 nanostructures obtained after anodization as the working electrode, an Ag/AgCl (3 M KCl) electrode as the reference electrode, and a platinum tip as the counter electrode. In order to check the Li insertion in the nanostructures, X-ray photoelectron spectroscopy (XPS) data were collected on a SPECS spectrometer equipped with a 150-MCD-9 detector and using a non-monochromatic Al Kα (1486.6

eV) X-ray source. Spectra were recorded at 175 °C, using an analyzer pass energy of 30 eV, an X-ray power of 50 W and under an operating pressure of 10^{-9} mbar.

For the electrochemical and photoelectrochemical tests, an electrochemical cell with the same electrodes and electrode configuration than that used for doping the samples was employed. In this case, due to the configuration of the photoelectrochemical cell, the area of the TiO_2 nanostructures exposed to the test solution was 0.13 cm^2. The electrochemical measurements (Electrochemical Impedance Spectroscopy (EIS) and Mott-Schottky analysis (M-S)) were conducted in a 0.1 M Na_2SO_4 solution using an Autolab PGSTAT302N potentiostat under dark conditions (without irradiation). EIS experiments were conducted at the open circuit potential (OCP) over a frequency range from 100 kHz to 10 mHz with a 10 mV (peak to peak) signal amplitude. Mott–Schottky plots were subsequently obtained by sweeping the potential from the OCP in the negative direction at 10 mV s^{-1} with an amplitude signal of 10 mV at a frequency value of 10 kHz.

The photoelectrochemical experiments were carried out under simulated sunlight condition AM 1.5 (100 $mW \cdot cm^{-2}$) in a 1M KOH solution. Photocurrent densities vs. potential curves were recorded by scanning the potential from −0.8 $V_{Ag/AgCl}$ to +0.5 $V_{Ag/AgCl}$ with a scan rate of 2 $mV \cdot s^{-1}$ and by chopped light irradiation (60 s in the dark and 20 s in the light). In order to evaluate the resistance of the nanostructures to photocorrosion, they were left at +0.5 $V_{Ag/AgCl}$ under illumination for one hour.

3. Results and discussion

3.1. Current density transients during anodization

Figure 2 shows the current density transients obtained during the potentiostatic anodization of Ti at 30 V at different Reynolds. In all cases, anodization curves present three stages. In stage I, current density decreases due to the fast formation of an insulating compact oxide layer (TiO_2) on titanium [43,47,54]. In the second stage (stage II), irregular nanoscale pores are formed due to the dissolution of this initial compact oxide film by the action of fluoride ions, which results in a current density increase to a maximum [47,55] and a subsequent decrease, due to the formation of the nanotubes. The third stage (stage III) is characterized by a progressive increase of the current density, which is related to the formation and growth of a regular nanostructured layer and the establishment of an equilibrium between field assisted oxide formation and dissolution [31,34,43,47,56]. It can be observed that, in general, there is a tendency for the slope of stage II to increase with increasing Re (especially at Re = 600), indicating that hydrodynamic conditions favor the diffusion of fluorides [45].

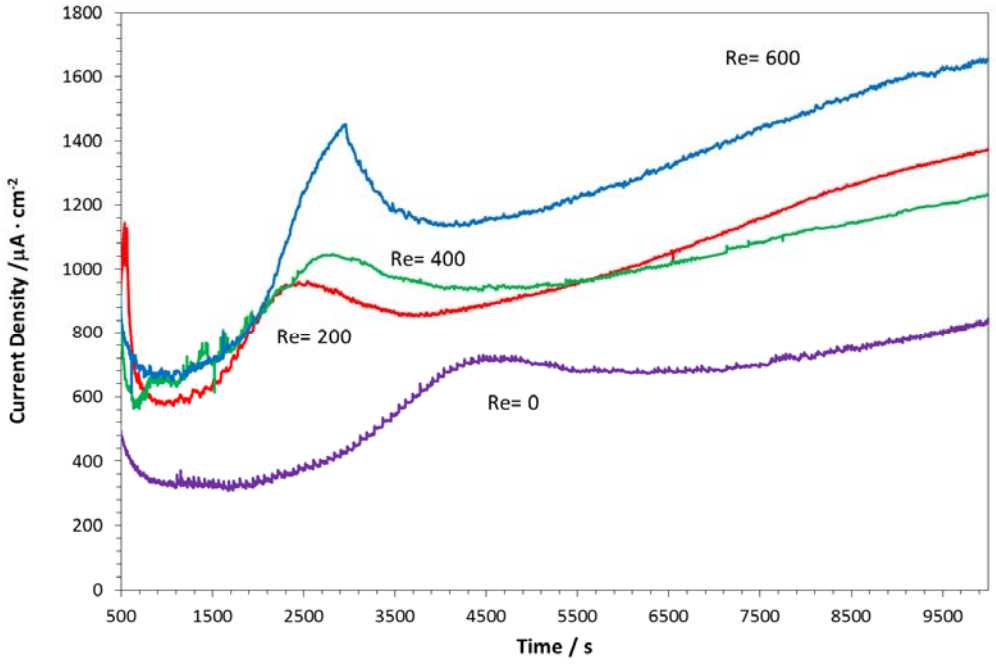

Figure 2. Current density transients obtained during the anodization of Ti at 30 V at different Reynold numbers (Re=0, Re=200, Re=400, Re=600).

3.2. Field Emission Scanning Electron Microscopy (FE-SEM)

Figure 3 shows the Field Emission Scanning Electron Microscope (FE-SEM) images of the samples obtained by electrochemical anodization of TiO_2 under static and hydrodynamic conditions and doped with Li^+. **Figure 3** allows distinguishing the top of self-organized TiO_2 nanotubes at Re=0. However, a different structure was observed under hydrodynamic conditions (Re > 0). As an example, **Figure 3** shows the top surface of the nanostructure formed at Re=600. This nanostructure is called nanosponge and is characterized by a connected and highly porous TiO_2 structure [34,43,44].

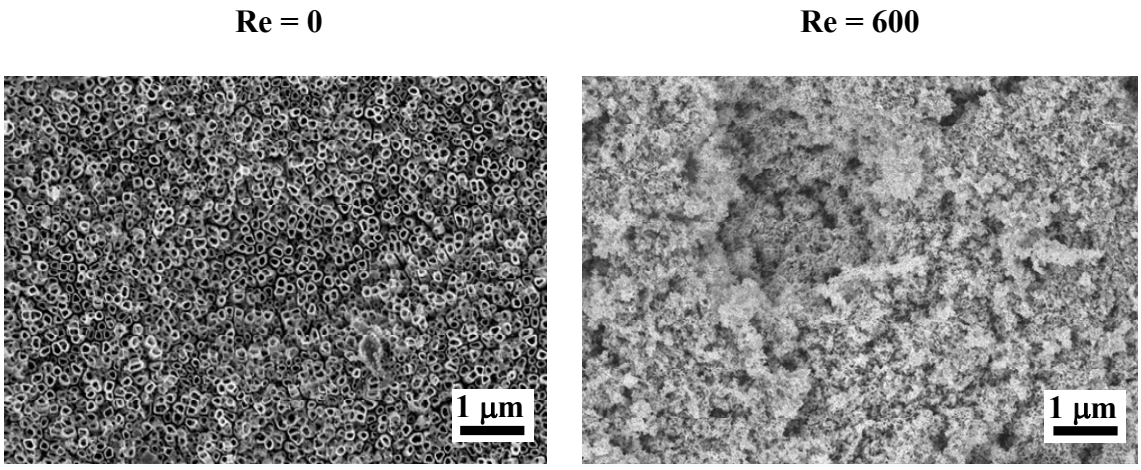

Figure 3. Field Emission Scanning Electron Microscope (FE-SEM) images of the samples obtained by electrochemical anodization of Li-doped TiO_2 under static (Re=0) and hydrodynamic conditions (Re=600).

Apart from a higher porosity, the nanosponge morphology obtained at Re > 0 implied an increase in the nanostructure layer thickness [43]. Hence, from FE-SEM images, it can be said that nanosponges have higher surface areas than nanotubes, which has a direct relation with subsequent Li^+ insertion.

The images shown in **Figure 3** are similar to those obtained by the authors in previous works [43] for anatase TiO_2 nanostructures under the same conditions of anodization but without Li^+ insertion. Therefore, the insertion of Li^+ does not reveal any significant change in the surface morphology of the nanostructures.

3.3. Raman Confocal Laser Microscopy

Figure 4 shows the Raman confocal laser spectra of the as-prepared and annealed TiO_2 nanostructures anodized at Re=0 and Re=600 and doped with Li^+; no differences were found in these spectra regardless of the Re used during anodization. Raman peaks originated from the molecular bond provide useful information about the crystallinity of the nanostructures. The as-prepared nanostructures show a single baseline, but it is not possible to distinguish defined peaks in their spectra. However, the annealed nanostructures show four peaks in the spectra at 149, 398, 516 and 637 cm^{-1}, which are typical of the anatase phase [57–61]. This fact indicates that the as-prepared samples are amorphous, but after the annealing process they present an anatase crystalline phase. Comparing these results with those obtained by the authors in previous works [43] for anatase TiO_2 nanostructures under the same anodization conditions but without Li^+ insertion, no changes were observed in the Raman spectra after Li^+ insertion. Therefore,

it can be concluded that there are no significant variations in the crystalline structure after Li^+ insertion.

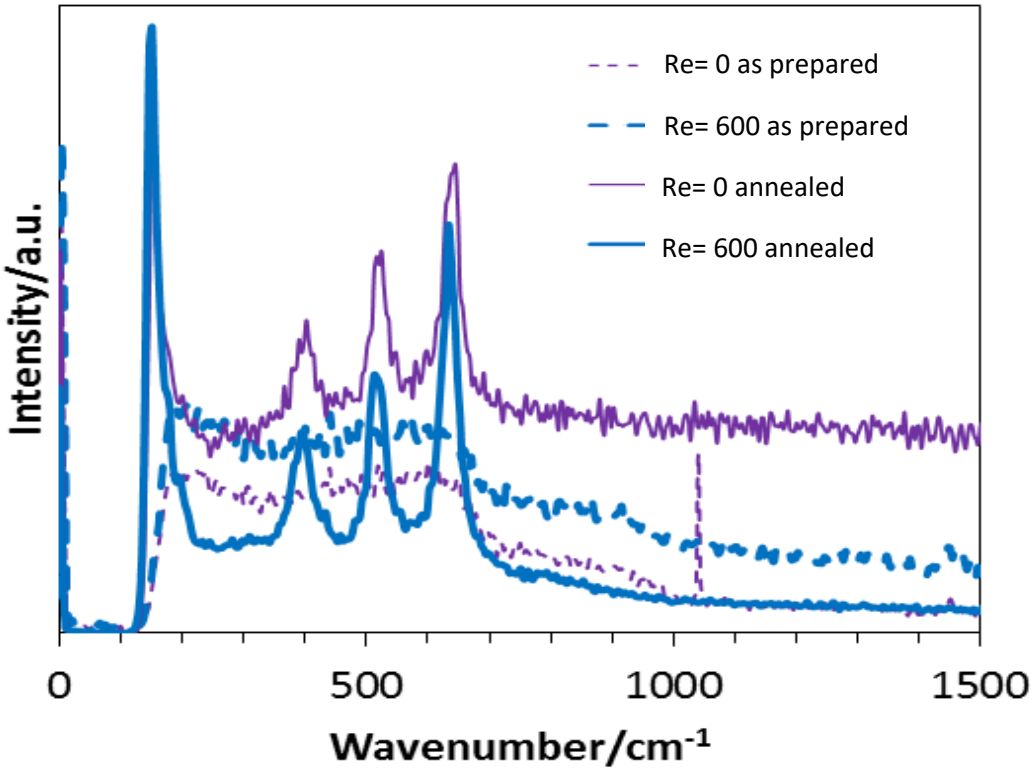

Figure 4. Raman confocal laser spectra of the as-prepared and annealed at 450 ºC during 1 hour Li-doped TiO_2 nanostructures obtained at Re=0 and Re=600.

3.4. XPS measurements

Figure 5a shows as an example the XPS spectrum of a Li-doped nanostructure anodized at Re = 600 and annealed at 450ºC for 1h.

The peak at ~55 eV of Li 1s spectrum was detected, as shown in **Figure 5b**, which indicates the successful Li doping. Additionally, the peak at ~61.5 eV corresponds to Ti 3s (**Figure 5b**). This confirms the presence of Ti^{3+} in the doped nanostructures, i.e. the intercalation of Li+ induces a partial reduction of Ti^{4+} to Ti^{3+} within the TiO_2 lattice [62].

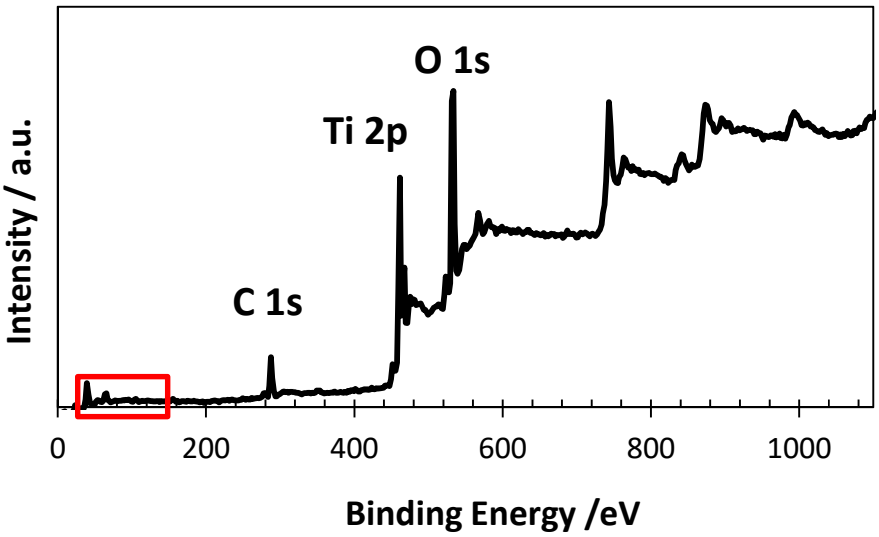

a)

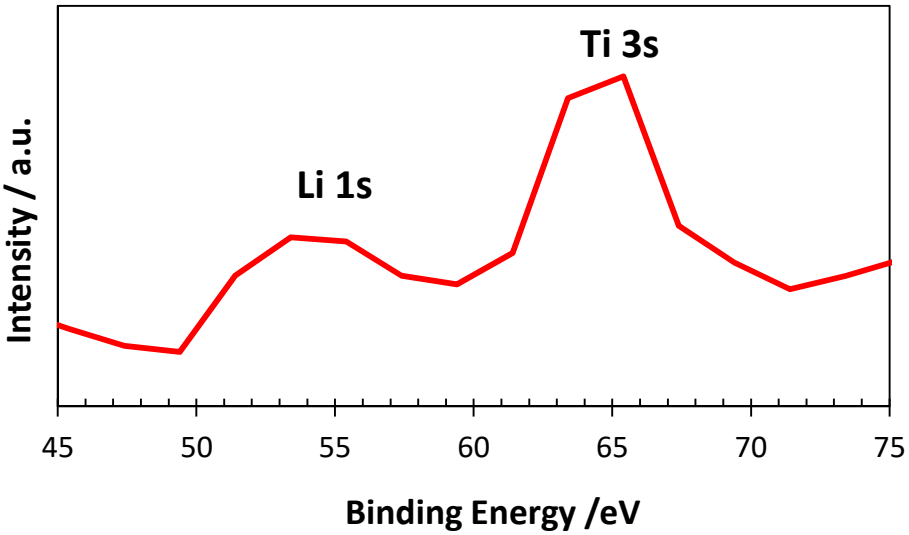

b)

Figure 5. XPS spectrum of the Li-doped TiO_2 nanostructure anodized at Re = 600 and annealed at 450 ºC during 1 h (a) and magnification of the XPS spectrum at the Li 1s peak region (b).

3.5. EIS measurements

Figure 6 shows the experimental Nyquist (**Figure 6a**), Bode-phase (**Figure 6b**) and Bode-module (**Figure 6c**) plots for the Li-doped TiO_2 nanostructures anodized at different Reynolds numbers, measured in a 0.1M Na_2SO_4 solution at open circuit potential under dark conditions and at 25º C.

Nyquist plots (**Figure 6a**) are characterized by an unfinished semicircle with high amplitude. On the other hand, Bode-phase plots (**Figure 6b**) show the presence of two well-defined time constants. This behavior could be associated with the formation of the nanostructure on the top of the compact TiO_2 layer [33].

Bode-module plots (**Figure 6c**) show lower values of impedance modules in nanosponges (anodized at Re > 0) than in nanotubes (anodized at Re=0) at low and intermediate frequencies, indicating that the anodization process under hydrodynamic conditions favors the conductivity of nanosponges. However, no differences are observed at high frequencies. This is due to the fact that the impedance at high frequencies in Bode plots corresponds to the resistance of the electrolyte which possesses similar values regardless of the Reynolds number.

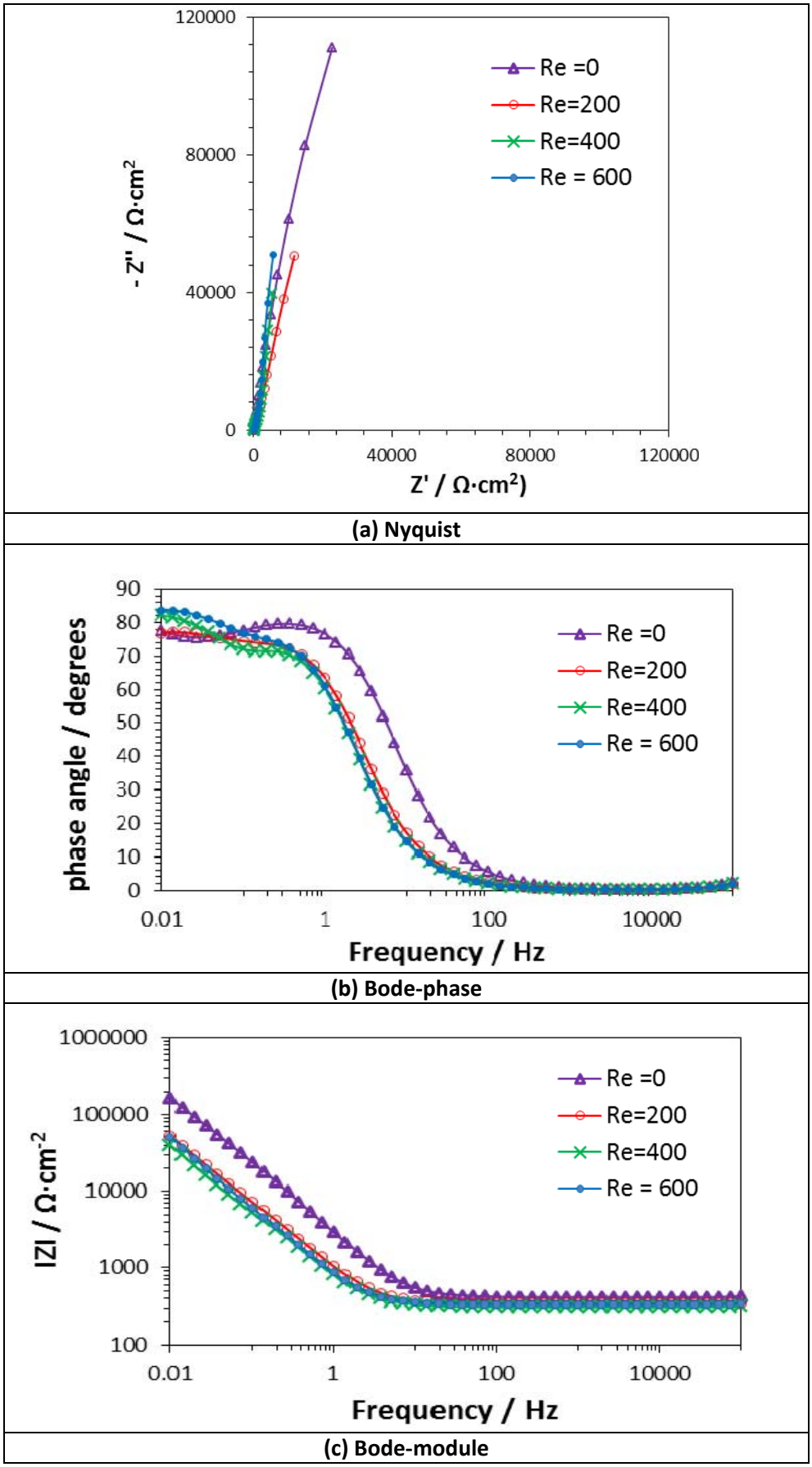

Figure 6. Experimental Nyquist (a), Bode-phase (b) and Bode-module (c) plots for the Li-doped samples anodized at different Reynolds numbers.

Experimental EIS data can be represented with the electrical equivalent circuit shown in **Figure 7.** This equivalent circuit has been used in the literature to model the impedance data of compact and nanoporous TiO_2 films [23,25,28,33,43,63]. Constant phase elements (CPEs) have been used instead of pure capacitors to account for frequency dispersion and non-ideality. This equivalent circuit is formed by a resistive element (R_s), corresponding to the electrolyte resistance, and two groups of resistances and constant phase elements (R-CPE), corresponding to the nanostructure overlayer (R_1-CPE_1) and the compact TiO_2 underlayer (R_2-CPE_2). CPEs have been converted into pure capacitances (C) by using the following equation [64, 65]:

$$C = \frac{(Q \cdot R)^{1/\alpha}}{R} \qquad \textbf{(2)}$$

where Q is the impedance of the CPE and R corresponds to R_2 when equation **(2)** is used to calculate C_2. To determine C_1 from CPE_1, R is calculated using equation **(3)**.

$$\frac{1}{R} = \frac{1}{R_S} + \frac{1}{R_1} \qquad \textbf{(3)}$$

The values of the equivalent circuit parameters obtained after fitting the EIS experimental results are shown in **Table 1**. R_s corresponds to the electrolyte resistance and it has similar values for all the studied conditions, since the electrolyte did not change. On the other hand, R_2 values are significantly higher than R_1 values regardless of the hydrodynamic conditions. This fact results from the higher electrical conductivity of the nanostructure overlayer (nanotubes or nanosponges) compared to the base oxide, as a consequence of the higher surface area of the former [17,21,33,66-68].

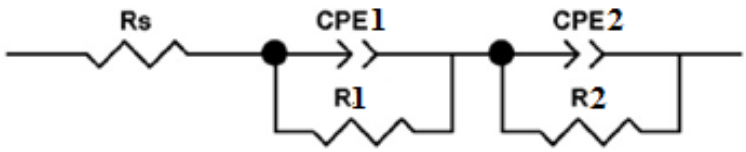

Figure 7. Electrical equivalent circuit used to simulate experimental EIS data.

Table 1. Equivalent circuit parameters for Li-doped TiO_2 nanostructures (nanotubes and nanosponges) at different Re values.

Re	**Rs** ($\Omega \cdot cm^2$)	**R_1** ($k\Omega \cdot cm^2$)	**C_1** ($\mu F \cdot cm^{-2}$)	**α_1**	**R_2** ($k\Omega \cdot cm^2$)	**C_2** ($\mu F \cdot cm^{-2}$)	**α_2**	**X^2** ($x10^{-4}$)
0	51.94 ± 2	3.20 ± 0.8	885 ± 25	0.90 ± 0.05	272.20 ± 5	835 ± 63	1.00 ± 0.05	2.2
200	43.23 ± 6	0.18 ± 0.1	7930 ± 180	0.97 ± 0.03	108.63 ± 9	3139 ± 201	0.91 ± 0.01	1.6
400	39.09 ± 5	0.36 ± 0.2	3660 ± 273	0.88 ± 0.02	77.41 ± 2	3192 ± 208	1.00 ± 0.02	2.7
600	41.81 ± 8	0.33 ± 0.3	4230 ± 123	0.85 ± 0.01	88.52 ± 7	2437 ± 255	1.00 ± 0.03	1.4

The CPE constant, α, indicates the ideality of the capacitive behavior of the CPE. **Table 1** shows that both α_1 and α_2 take values around 1 in all cases, in general α_1 values being lower than α_2. This implies that the TiO_2 nanostructure overlayer has a higher active

surface and is more heterogeneous, that is, this overlayer is more conductive and defective in comparison to the compact TiO_2 underlayer, whose behavior approximates to an ideal capacitor [33,43,63].

Additionally, C_1 values are higher than C_2 values in all cases (**Table 1**). This fact can be attributed to a lower thickness of the TiO_2 nanostructure overlayer or to a higher porosity of this layer as compared to the compact TiO_2 underlayer. Even these higher C_1 values have been associated with a higher density of charge carriers by other authors to [69].

With respect to the behavior of the different doped nanostructures obtained in this work depending on the hydrodynamic conditions of the anodization process, **Table 1** shows that R_1 values are higher for the nanotubes formed under static conditions than for the nanosponges formed at Re > 0, indicating that the electrical conductivity of the TiO_2 nanosponges is higher in comparison to that of the TiO_2 nanotubes. R_2 values are also higher for nanotubes, indicating that the hydrodynamic conditions also affect the electrical properties of the compact TiO_2 underlayer. In general, α_1 values are lower in the case of Re≠0 than in the case of Re > 0, indicating a higher degree of porosity in the nanosponges formed under hydrodynamic conditions compared with the nanotubes formed with Re = 0, which confirms the R_1 results. Similarly, C_1 and C_2 are higher in the nanosponges than in the nanotubes, indicating that nanosponges have a higher density of charge carriers.

Comparing with the results obtained by the authors in previous works [43] for anatase TiO_2 nanostructures under the same anodization conditions but without Li^+ insertion, it can be concluded that doping with Li^+ significantly reduces the resistance of both the

TiO_2 nanostructure overlayer and the compact TiO_2 underlayer in all studied conditions (Re=0 and Re > 0), since higher values of R_1 and R_2 were obtained for the undoped nanostructures. As an example, R_1 and R_2 values at Re=0 were around 9 $\Omega \cdot cm^2$ and 576 $\Omega \cdot cm^2$ respectively and for the Re= 400 around 2 $\Omega \cdot cm^2$ and 860 $\Omega \cdot cm^2$ respectively (undoped nanosponges) [43]. Additionally, higher values of both C_1 and C_2 were obtained for the doped nanostructures than for the undoped ones, indicating a higher density of charge carriers in the doped nanotubes and nanosponges [69]. These facts can be explained by a higher number of controlled defects due to Li^+ insertion which improves conductivity.

3.5 Mott-Schottky analysis

Figure 8 shows the Mott Schottky plots of the Li-doped nanostructures formed at different Reynolds numbers. These plots have been obtained under dark conditions and at a frequency of 10 kHz since at this high value there is no capacitance dependence on frequency [70-72] and the measured capacitance can be entirely attributed to the space charge capacitance [73]. The Mott-Schottky analysis is a common tool used for the characterization of the electrochemical capacitance of the semiconductor/electrolyte interface as a function of the applied potential [23].

In this analysis, the total capacitance can be approximated by the capacitance of the depleted semiconductor electrode, which is known as the space charge capacitance (C_{SC}). The Mott-Schottky equation (**eq.4**) for an n-type semiconductor (such as TiO_2) predicts a linear relationship of C_{SC}^{-2} with the applied potential (U) [33, 73]:

$$\frac{1}{C_{SC}^{\ 2}} = \left(\frac{2}{e \cdot \varepsilon_0 \cdot \varepsilon_r \cdot N_D}\right) \cdot \left(U - U_{FB} - \frac{k \cdot T}{e}\right) \quad \textbf{(4)}$$

where N_D is the donor density, ε_0 ($8.85 \cdot 10^{-14}$ F/cm) the vacuum permittivity, ε_r the dielectric constant, e the electron charge ($1.60 \cdot 10^{-19}$ C), U_{FB} the flatband potential, k the Boltzmann constant ($1.38 \cdot 10^{-23}$ J/K) and T is the absolute temperature. The dielectric constant varies depending on the Li^+ insertion, taking a value of 500 for doped TiO_2 nanostructures [49]. In fact, Van de Krol et al. claimed that the increase in the dielectric constant may be originated by an increase in the polarizability of the TiO_2 from the inserted Li^+ cations [73].

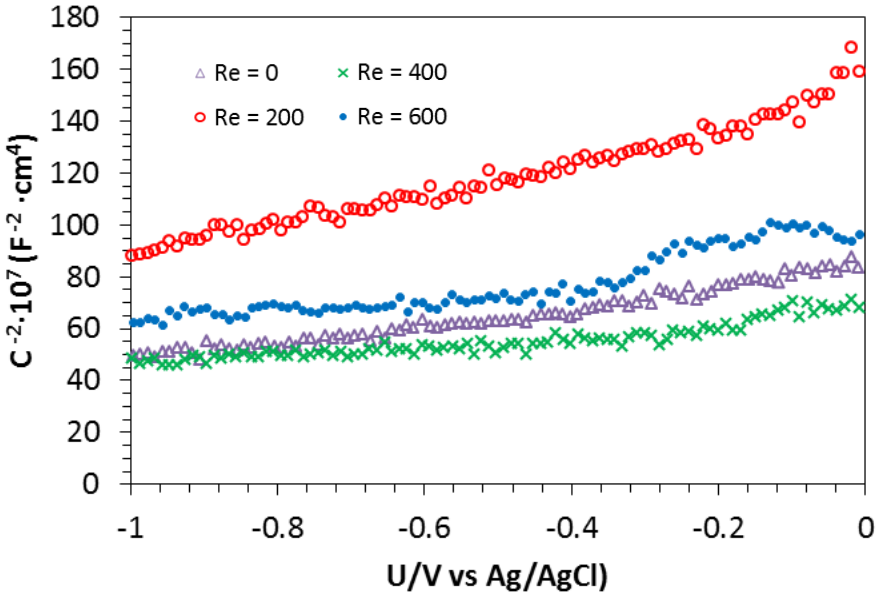

Figure 8. Mott Schottky plots obtained at a frequency of 10 kHz for the Li-doped nanostructures formed at different Reynolds numbers.

The positive slopes of the M-S plots (**Figure 8**) are characteristics of *n*-type semiconductors, with the dominant defects in TiO_2 being oxygen vacancies due to their lower formation energy compared with Ti^{3+} interstitials [34,65,74-79]. The donor

densities (N_D) can be determined from the positive slopes of the straight lines in the Mott-Schottky plots using **eq. 4** (**Table 2**).

Table 2. Values of N_D and U_{FB} for Li-doped TiO_2 nanostructures (nanotubes and nanosponges) at different Re values.

Re	N_D (x 10^{21} cm^{-3})	U_{FB} (V $_{vs\ (Ag/AgCl)}$)
0	3.61	-3.10
200	4.38	-2.34
400	13.00	-4.36
600	18.00	-6.82

The donor density of the doped nanostructures increases as Reynolds number increases (**Table 2**). That is, nanosponges have a higher value of donor density than nanotubes. The increase in oxygen vacancies should improve the n-type character of the TiO_2 nanostructures and thus enhance electron transport through the nanostructures [18,19,66]. However, although this fact seems to be a favorable effect due to an increase in the electrical conductivity of the nanostructure, it can also be related to a decrease in thickness of the depletion layer, resulting in an increase of the recombination losses [70,72,80]. If the depletion layer is very thin, photons can penetrate beyond this layer and light will be absorbed in the bulk semiconductor, where the electrical field is absent [43,70,72,80-81]. The lack of an electrical field prevents the photo-excited electron-hole pairs from being effectively separated, thus increasing the probability of recombination [33,70,72,80]. Moreover, oxygen vacancies in TiO_2 can act as recombination centers for electron and holes, leading to a decrease in the efficiency of the photocatalytic process

since they play a critical role in the trapping process: an excess of oxygen vacancies will result in more trapped photogenerated electrons thus decreasing their contribution to the photoelectrochemical processes [19,82,83].

Comparing the results obtained in this study with the results obtained by the authors in previous works [43] for undoped anatase TiO_2 nanostructures under the same anodization conditions, it can be concluded that the donor density notably increases in the doped samples compared to the undoped ones. This increase in the donor density might be associated with an increase in the number of defects present in the TiO_2 nanostructures due to Li^+ insertion. These defects improve charge transfer through the nanostructures, which is in agreement with the results obtained by EIS.

The recombination probability can also be affected by the flatband potential (U_{FB}),which is the potential required to reduce band bending of the semiconductor to zero, i.e., at this potential there is no depleted space charge layer. The U_{FB} value is related to the potential drop at the depletion space charge layer, $U_{SC,}$, and the applied external potential, U, according to **eq. 5**:

$$U_{SC} = U - U_{FB} \quad \textbf{(5)}$$

According to **eq. 5**, assuming a constant value of U, the higher and more negative the value of U_{FB}, the higher the value of U_{SC} and, consequently, the stronger the electrical field within the depleted space charge layer, which is the driving force to separate the photogenerated electron-hole pairs. Thus, to favor charge separation and reduce recombination probability U_{FB} should be high and negative [19,70].

Table 2 shows the U_{FB} values obtained from the intercept of the straight line with the potential axis in the M-S plot [72]. The most negative U_{FB} values were obtained at Re=400 and Re= 600, indicating a displacement of the Fermi level towards the conduction band edge and, consequently, to a larger band bending and electrical field within the depleted space charge layer [18,19,66]. These results indicate that the recombination probability diminishes as the Reynolds number increases in the case of the nanosponges.

Comparing these results with the results obtained by the authors in previous works [43] for undoped anatase TiO_2 nanostructures under the same anodization conditions, it can be concluded that flatband potential is more negative in the Li-doped TiO_2 nanostructures than in the undoped ones, which indicates that Li^+ insertion favors charge separation and reduces recombination probability.

3.6. Photoelectrochemical tests

Figure 9 shows the photoelectrochemical tests carried out under simulated sunlight AM 1.5 conditions for the Li-doped nanostructures formed at different Reynolds numbers. It can be observed that photocurrent densities increase with Reynolds number, showing the highest increase when Reynolds increases from 200 to 400. This fact indicates that, on the one hand, nanosponges of anatase TiO_2 (Re > 0) generate higher photocurrent densities than nanotubes (Re=0) when used as photocatalyst in water splitting. This is in agreement with the EIS measurements (lower R_1 values for nanostructures obtained under hydrodynamic conditions) and with the Mott-Schottky analysis (higher values of

the donor density and flatband potentials (in absolute value) obtained under hydrodynamic conditions). On the other hand, the performance of these nanosponges improves as the hydrodynamic conditions during anodization increase, which is also in agreement with the EIS and Mott-Schottky measurements. The high photocurrent densities obtained for the nanostructures anodized at higher Reynolds numbers are related to an increase in their conductivity, which favors the current flow [28,82].

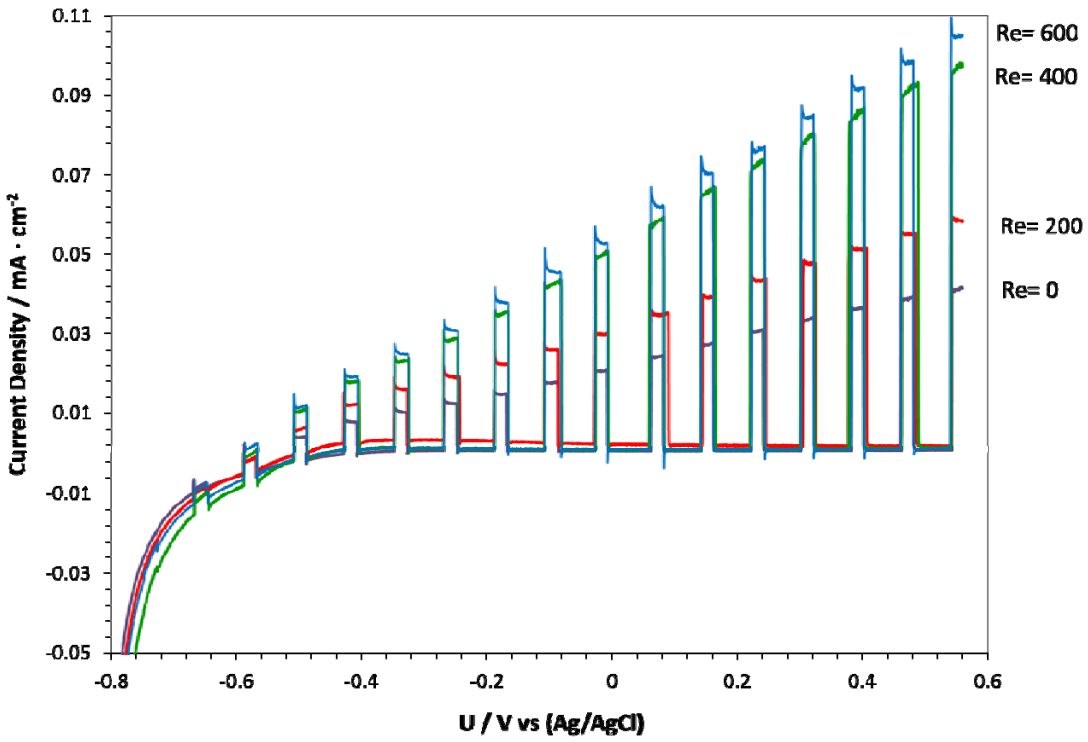

Figure 9. Photoelectrochemical water splitting tests carried out under simulated sunlight AM 1.5 conditions for the Li-doped nanostructures formed at different Reynolds numbers.

Comparing the results shown in **Figure 9** with the results obtained by the authors in previous works [43] for undoped anatase TiO_2 nanostructures under the same anodization conditions, it can be concluded that doping with Li^+ increases the photocurrent registered during water splitting, especially at higher Reynolds numbers.

As an example, values around 0.1 mA/cm^2 were reached for the Li-doped nanosponges synthesized at Re=400 while values around 0.07 mA/cm^2 were reached for the undoped nanosponges synthesized under the same conditions [43]. This result is in agreement with the increase in the conductivity of the Li-doped nanostructures: lower R_1 and R_2 in the doped nanostructures than in the undoped ones, as well as an increase in donor density and flatband potentials (in absolute value) for the doped nanostructures. In general, cation insertion into the nanostructures can reduce the recombination losses associated with the capture of electrons by trap states, which mainly originate from incompletely coordinated Ti^{+4} surface sites [49,73,83,84-88]. Hence, the blocking of these charge recombination sites could be the cause of the photocurrent enhancement of the Li^+ doped samples.

3.6. Stability against photocorrosion

It is important to check if the nanostructures obtained in this work are stable agaisnt photocorrosion. **Figure 10** shows the photostability experiments carried out under AM 1.5 illumination at 0.5 $V_{Ag/AgCl}$ during 1 hour in 1 M KOH solution for the samples anodized at different Reynolds numbers and doped with Li^+. Results show that both nanotubes and nanosponges registers of photocurrent densities are stable with time, i.e., they are stable to photocorrosion and the Li^+ doping process is stable.

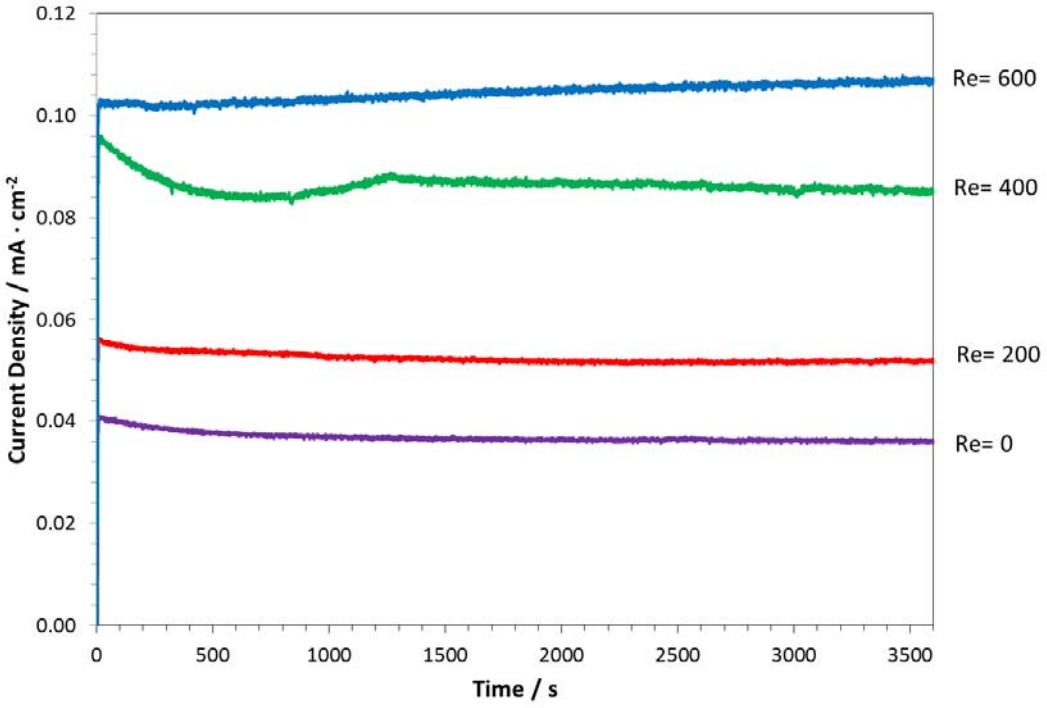

Figure 10. Photostability experiments carried out under AM 1.5 illumination at 0.5 $V_{Ag/AgCl}$ of the Li-doped samples anodized at different Reynolds numbers.

4. Conclusions

The morphology of the TiO_2 nanostructures formed by Ti anodization in glycerol/water electrolytes with fluorides depended on the hydrodynamic conditions during anodization: nanotubes were formed under static conditions and nanosponges were formed under hydrodynamic conditions. FE-SEM images showed these different nanostructures.

Li-doped nanosponges of anatase TiO_2 (Re > 0) generated higher photocurrent densities than nanotubes (Re=0) when they were used as photocatalysts. This is in agreement

with the EIS measurements (lower impedance, R_1 and α_1 values for nanostructures obtained under hydrodynamic conditions), indicating that the anodization process under hydrodynamic conditions favored the conductivity of the formed nanostructure, as well as a higher degree of porosity in nanosponges than in nanotubes. The Mott-Schottky measurements also corroborated this behavior, with higher values of donor density and flatband potentials (in absolute value) under hydrodynamic conditions, indicating a lower recombination probability in nanosponges than in nanotubes.

The performance of nanosponges improved as the hydrodynamic conditions during anodization increased, which is also in agreement with the EIS and Mott- Schottky measurements. The high photocurrent densities obtained for the nanosponges anodized at higher Reynolds numbers were related to an increase of their conductivity and to a decrease in their recombination probability, which favored the current flow.

Comparing the results obtained in this study with the results obtained by the authors in previous works, it was observed that doping with Li^+ significantly diminished the resistance of both TiO_2 nanostructures, increasing their conductivity. Both the donor density and the flatband potential (in absolute value) notably increased in the Li-doped samples compared to the undoped ones, which might be associated with an increase in the number of defects present in the TiO_2 nanostructures due to Li^+ insertion. These defects improved charge transfer through the nanostructures. In general, Li cation insertion into the nanostructures seemed to reduce the recombination losses associated with the capture of electrons by trap states. Moreover, doping with Li^+ increased the photocurrent registered during water splitting, especially at higher Reynolds numbers.

Results showed that both nanotubes and nanosponges registered stable photocurrent densities with time, i.e., they were resistant to photocorrosion and the Li^+ doping process was stable.

Acknowledgements: Authors thank for the financial support to the Ministerio de Economía y Competitividad (Project Code: CTQ2016-79203-R), for its help in the Laser Raman Microscope acquisition (UPOV08-3E-012), and for the co-finance by the European Social Fund.

REFERENCES

[1] A. Fujishima, X. Zhang, D. Trick, TiO2 photocatalysis and related surface phenomena, Surface Science Reports. 63 (2008) 515–582. doi:10.1016/j.surfrep.2008.10.001.

[2] K. Maeda, K. Domen, Photocatalytic Water Splitting: Recent Progress and Future Challenges, The Journal of Physical Chemistry Letters. 1 (2010) 2655–2661. doi:10.1021/jz1007966.

[3] J.M. Macak, M. Zlamal, J. Krysa, P. Schmuki, Self-Organized TiO2 Nanotube Layers as Highly Efficient Photocatalysts, Small. 3 (2007) 300–304. doi:10.1002/smll.200600426.

[4] P. Roy, D. Kim, K. Lee, E. Spiecker, P. Schmuki, J. Desilvestro, et al., TiO2 nanotubes and their application in dye-sensitized solar cells, Nanoscale. 2 (2010) 45–59. doi:10.1039/B9NR00131J.

[5] A. Fujishima, T.N. Rao, D.A. Tryk, Titanium dioxide photocatalysis, Journal of Photochemistry and Photobiology C: Photochemistry Reviews. 1 (2000) 1–21. doi:10.1016/S1389-5567(00)00002-2.

[6] J.H. Park, S. Kim, A.J. Bard, Novel Carbon-Doped TiO_2 Nanotube Arrays with High Aspect Ratios for Efficient Solar Water Splitting, Nano Letters. 6 (2006) 24–28. doi:10.1021/nl051807y.

[7] J. Park, S. Bauer, K. von der Mark, P. Schmuki, Nanosize and Vitality: TiO_2 Nanotube Diameter Directs Cell Fate, Nano Letters. 7 (2007) 1686–1691. doi:10.1021/nl070678d.

[8] X. Chen, L. Liu, P.Y. Yu, S.S. Mao, Increasing Solar Absorption for Photocatalysis with Black Hydrogenated Titanium Dioxide Nanocrystals, Science 331 (2011) 746-750.

doi: 10.1126/science.1200448

[9] T. Xia, Y. Zhang, J. Murowchick, X. Chen, Vacuum-treated titanium dioxide nanocrystals: Optical properties, surface disorder, oxygen vacancy, and photocatalytic activities, Catalysis Today 225 (2014) 2-9.
doi: 10.1016/j.cattod.2013.08.026

[10] X. Chen, M. Schriver, T. Suen, S.S. Mao, Fabrication of 10 nm diameter TiO2 nanotube arrays by titanium anodization, Thin Solid Films 515 (2007) 8511-8514.
doi: 10.1016/j.tsf.2007.03.110

[11] C. Ampelli, F. Tavella, S. Perathoner, G. Centi, Engineering of photoanodes based on ordered TiO2-nanotube arrays in solar photo-electrocatalytic (PECa) cells, Chemical Engineering Journal 320 (2017) 352-362.
doi: 10.1016/j.cej.2017.03.066

[12] M.R. Hoffmann, S.T. Martin, W. Choi, D.W. Bahnemann, Environmental Applications of Semiconductor Photocatalysis, Chemical Reviews. 95 (1995) 69–96. doi:10.1021/cr00033a004.

[13] M. Adachi, Y. Murata, M. Harada, S. Yoshikawa, Formation of Titania Nanotubes with High Photo-Catalytic Activity., Chemistry Letters. (2000) 942–943. doi:10.1246/cl.2000.942.

[14] T. Sreethawong, Y. Suzuki, S. Yoshikawa, Photocatalytic evolution of hydrogen over nanocrystalline mesoporous titania prepared by surfactant-assisted templating sol–gel process, Catalysis Communications. 6 (2005) 119–124. doi:10.1016/j.catcom.2004.11.011.

[15] C.-C. Tsai, J.-N. Nian, H. Teng, Mesoporous nanotube aggregates obtained from hydrothermally treating TiO2 with NaOH, Applied Surface Science. 253 (2006)

1898–1902. doi:10.1016/j.apsusc.2006.03.035.

[16] I. Paramasivam, H. Jha, N. Liu, P. Schmuki, A Review of Photocatalysis using Self-organized TiO 2 Nanotubes and Other Ordered Oxide Nanostructures, Small. 8 (2012) 3073–3103. doi:10.1002/smll.201200564.

[17] D. D'Elia, C. Beauger, J.-F. Hochepied, A. Rigacci, M.-H. Berger, N. Keller, et al., Impact of three different TiO2 morphologies on hydrogen evolution by methanol assisted water splitting: Nanoparticles, nanotubes and aerogels, International Journal of Hydrogen Energy. 36 (2011) 14360–14373. doi:10.1016/j.ijhydene.2011.08.007.

[18] L. Yu, Z. Wang, L. Shi, S. Yuan, Y. Zhao, J. Fang, et al., Photoelectrocatalytic performance of TiO2 nanoparticles incorporated TiO2 nanotube arrays, Applied Catalysis B: Environmental. 113 (2012) 318–325. doi:10.1016/j.apcatb.2011.12.004.

[19] D. Wang, X. Zhang, P. Sun, S. Lu, L. Wang, C. Wang, et al., Photoelectrochemical Water Splitting with Rutile TiO2 Nanowires Array: Synergistic Effect of Hydrogen Treatment and Surface Modification with Anatase Nanoparticles, Electrochimica Acta. 130 (2014) 290–295. doi:10.1016/j.electacta.2014.03.024.

[20] A. Wolcott, W.A. Smith, T.R. Kuykendall, Y. Zhao, J.Z. Zhang, Photoelectrochemical Water Splitting Using Dense and Aligned TiO 2 Nanorod Arrays, Small. 5 (2009) 104–111. doi:10.1002/smll.200800902.

[21] G. Wang, H. Wang, Y. Ling, Y. Tang, X. Yang, R.C. Fitzmorris, et al., Hydrogen-Treated TiO 2 Nanowire Arrays for Photoelectrochemical Water Splitting, Nano Letters. 11 (2011) 3026–3033. doi:10.1021/nl201766h.

[22] J.M. Macak, H. Tsuchiya, A. Ghicov, K. Yasuda, R. Hahn, S. Bauer, et al., TiO2

nanotubes: Self-organized electrochemical formation, properties and applications, Current Opinion in Solid State and Materials Science. 11 (2007) 3–18. doi:10.1016/j.cossms.2007.08.004.

[23] A.G. Muñoz, Semiconducting properties of self-organized TiO2 nanotubes, Electrochimica Acta. 52 (2007) 4167–4176. doi:10.1016/j.electacta.2006.11.035.

[24] P. Pillai, K.S. Raja, M. Misra, Electrochemical storage of hydrogen in nanotubular TiO2 arrays, Journal of Power Sources. 161 (2006) 524–530. doi:10.1016/j.jpowsour.2006.03.088.

[25] A.G. Muñoz, Q. Chen, P. Schmuki, Interfacial properties of self-organized TiO2 nanotubes studied by impedance spectroscopy, Journal of Solid State Electrochemistry. 11 (2007) 1077–1084. doi:10.1007/s10008-006-0241-9.

[26] H. Tsuchiya, J.M. Macak, A. Ghicov, A.S. Räder, L. Taveira, P. Schmuki, Characterization of electronic properties of TiO2 nanotube films, Corrosion Science. 49 (2007) 203–210. doi:10.1016/j.corsci.2006.05.009.

[27] S.K. Mohapatra, M. Misra, V.K. Mahajan, K.S. Raja, A novel method for the synthesis of titania nanotubes using sonoelectrochemical method and its application for photoelectrochemical splitting of water, Journal of Catalysis. 246 (2007) 362–369. doi:10.1016/j.jcat.2006.12.020.

[28] P. Xiao, D. Liu, B.B. Garcia, S. Sepehri, Y. Zhang, G. Cao, Electrochemical and photoelectrical properties of titania nanotube arrays annealed in different gases, Sensors and Actuators B: Chemical. 134 (2008) 367–372. doi:10.1016/j.snb.2008.05.005.

[29] F. Fabregat-Santiago, E.M. Barea, J. Bisquert, G.K. Mor, K. Shankar, C.A. Grimes, High Carrier Density and Capacitance in TiO_2 Nanotube Arrays Induced by Electrochemical Doping, Journal of the American Chemical Society.

130 (2008) 11312–11316. doi:10.1021/ja710899q.

[30] Z. Liu, B. Pesic, K.S. Raja, R.R. Rangaraju, M. Misra, Hydrogen generation under sunlight by self ordered TiO2 nanotube arrays, International Journal of Hydrogen Energy. 34 (2009) 3250–3257. doi:10.1016/j.ijhydene.2009.02.044.

[31] D. Wang, Y. Liu, B. Yu, F. Zhou, W. Liu, TiO 2 Nanotubes with Tunable Morphology, Diameter, and Length: Synthesis and Photo-Electrical/Catalytic Performance, Chemistry of Materials. 21 (2009) 1198–1206. doi:10.1021/cm802384y.

[32] T.-S. Kang, A.P. Smith, B.E. Taylor, M.F. Durstock, Fabrication of Highly-Ordered TiO 2 Nanotube Arrays and Their Use in Dye-Sensitized Solar Cells, Nano Letters. 9 (2009) 601–606. doi:10.1021/nl802818d.

[33] D.P. Oyarzún, R. Córdova, O.E. Linarez Pérez, E. Muñoz, R. Henríquez, M. López Teijelo, et al., Morphological, electrochemical and photoelectrochemical characterization of nanotubular TiO2 synthesized electrochemically from different electrolytes, Journal of Solid State Electrochemistry. 15 (2011) 2265–2275. doi:10.1007/s10008-010-1236-0.

[34] R. Sánchez-Tovar, K. Lee, J. García-Antón, P. Schmuki, Formation of anodic TiO2 nanotube or nanosponge morphology determined by the electrolyte hydrodynamic conditions, Electrochemistry Communications. 26 (2012) 1–4. doi:10.1016/j.elecom.2012.09.041.

[35] L. Aïnouche, L. Hamadou, A. Kadri, N. Benbrahim, D. Bradai, Interfacial Barrier Layer Properties of Three Generations of TiO2 Nanotube Arrays, Electrochimica Acta. 133 (2014) 597–609. doi:10.1016/j.electacta.2014.04.086.

[36] T. Kasuga, M. Hiramatsu, A. Hoson, T. Sekino, K. Niihara, Formation of Titanium Oxide Nanotube, Langmuir. 14 (1998) 3160–3163.

doi:10.1021/la9713816.

[37] J.H. Jung, H. Kobayashi, K.J.C. van Bommel, S. Shinkai, T. Shimizu, Creation of Novel Helical Ribbon and Double-Layered Nanotube TiO 2 Structures Using an Organogel Template, Chemistry of Materials. 14 (2002) 1445–1447. doi:10.1021/cm011625e.

[38] D.V. Bavykin, J.M. Friedrich, F.C. Walsh, Protonated Titanates and TiO2 Nanostructured Materials: Synthesis, Properties, and Applications, Advanced Materials. 18 (2006) 2807–2824. doi:10.1002/adma.200502696.

[39] D. V. Bavykin, V.N. Parmon, A.A. Lapkin, F.C. Walsh, The effect of hydrothermal conditions on the mesoporous structure of TiO2 nanotubes, Journal of Materials Chemistry. 14 (2004) 3370. doi:10.1039/b406378c.

[40] R. Sánchez-Tovar, I. Paramasivam, K. Lee, P. Schmuki, Influence of hydrodynamic conditions on growth and geometry of anodic TiO2 nanotubes and their use towards optimized DSSCs, Journal of Materials Chemistry. 22 (2012) 12792. doi:10.1039/c2jm31246h.

[41] V. Zwilling, E. Darque-Ceretti, A. Boutry-Forveille, D. David, M.Y. Perrin, M. Aucouturier, Structure and physicochemistry of anodic oxide films on titanium and TA6V alloy, Surface and Interface Analysis. 27 (1999) 629–637. doi:10.1002/(SICI)1096-9918(199907)27:7<629::AID-SIA551>3.0.CO;2-0.

[42] J.M. Macák, H. Tsuchiya, P. Schmuki, High-Aspect-Ratio TiO 2 Nanotubes by Anodization of Titanium, Angewandte Chemie International Edition. 44 (2005) 2100–2102. doi:10.1002/anie.200462459.

[43] R. Sánchez-Tovar, R.M. Fernández-Domene, D.M. García-García, J. García-Antón, Enhancement of photoelectrochemical activity for water splitting by controlling hydrodynamic conditions on titanium anodization, Journal of Power

Sources. 286 (2015) 224–231. doi:10.1016/j.jpowsour.2015.03.174.

[44] R. Sanchez-Tovar, K. Lee, J. Garcia-Anton, P. Schmuki, Photoelectrochemical Poperties of Anodic TiO_2 Nanosponge Layers, Ecs Electrochemistry Letters. 2 (2013) H9–H11. doi:Doi 10.1149/2.005303eel.

[45] J. Borràs-Ferrís, R. Sánchez-Tovar, E. Blasco-Tamarit, R.M. Fernández-Domene, J. García-Antón, Effect of Reynolds number and lithium cation insertion on titanium anodization, Electrochimica Acta. 196 (2016) 24–32. doi:10.1016/j.electacta.2016.02.160.

[46] A. Ghicov, P. Schmuki, Self-ordering electrochemistry: a review on growth and functionality of TiO2 nanotubes and other self-aligned MOx structures, Chemical Communications. (2009) 2791. doi:10.1039/b822726h.

[47] P. Roy, S. Berger, P. Schmuki, TiO2 Nanotubes: Synthesis and Applications, Angewandte Chemie International Edition. 50 (2011) 2904–2939. doi:10.1002/anie.201001374.

[48] R. Beranek, A. Tsuchiya, T.M. Sugishima, L. Macak, S. Taveira, Fujimoto, et al., Enhancement and limits of the photoelectrochemical response from anodic TiO2 nanotubes, Applied Physics Letters. 87 (2005) 1–3. doi:10.1063/1.2140085.

[49] L. Tsui, M. Saito, T. Homma, G. Zangari, Trap-state passivation of titania nanotubes by electrochemical doping for enhanced photoelectrochemical performance, Journal of Materials Chemistry A. 3 (2015) 360–367. doi:10.1039/C4TA05620E.

[50] J. Yang, X. Wang, X. Yang, J. Li, X. Zhang, J. Zhao, Energy storage ability and anti-corrosion properties of Bi-doped TiO2 nanotube arrays, Electrochimica Acta. 169 (2015) 227–232. doi:10.1016/j.electacta.2015.04.076.

[51] M.M. Momeni, Y. Ghayeb, Z. Ghonchegi, Fabrication and characterization of

copper doped TiO2 nanotube arrays by in situ electrochemical method as efficient visible-light photocatalyst, Ceramics International. 41 (2015) 8735–8741. doi:10.1016/j.ceramint.2015.03.094.

[52] R. Hahn, A. Ghicov, H. Tsuchiya, J.M. Macak, A.G. Muñoz, P. Schmuki, Lithium-ion insertion in anodic TiO 2 nanotubes resulting in high electrochromic contrast, Physica Status Solidi (a). 204 (2007) 1281–1285. doi:10.1002/pssa.200674310.

[53] J.M. Macak, B.G. Gong, M. Hueppe, P. Schmuki, Filling of TiO2 Nanotubes by Self-Doping and Electrodeposition, Advanced Materials. 19 (2007) 3027–3031. doi:10.1002/adma.200602549.

[54] K. Shankar, G.K. Mor, H.E. Prakasam, S. Yoriya, M. Paulose, O.K. Varghese, et al., Highly-ordered TiO 2 nanotube arrays up to 220 μm in length: use in water photoelectrolysis and dye-sensitized solar cells, Nanotechnology. 18 (2007) 065707. doi:10.1088/0957-4484/18/6/065707.

[55] D. Regonini, C.R. Bowen, A. Jaroenworaluck, R. Stevens, A review of growth mechanism, structure and crystallinity of anodized TiO2 nanotubes, Materials Science and Engineering: R: Reports. 74 (2013) 377–406. doi:10.1016/j.mser.2013.10.001.

[56] S.P. Albu, A. Ghicov, J.M. Macak, R. Hahn, P. Schmuki, Self-Organized, Free-Standing TiO 2 Nanotube Membrane for Flow-through Photocatalytic Applications, Nano Letters. 7 (2007) 1286–1289. doi:10.1021/nl070264k.

[57] L.L. Costa, A.G.S. Prado, TiO2 nanotubes as recyclable catalyst for efficient photocatalytic degradation of indigo carmine dye, Journal of Photochemistry and Photobiology A: Chemistry. 201 (2009) 45–49. doi:10.1016/j.jphotochem.2008.09.014.

[58] P.-T. Hsiao, K.-P. Wang, C.-W. Cheng, H. Teng, Nanocrystalline anatase TiO2 derived from a titanate-directed route for dye-sensitized solar cells, Journal of Photochemistry and Photobiology A: Chemistry. 188 (2007) 19–24. doi:10.1016/j.jphotochem.2006.11.013.

[59] L. Qian, Z.-L. Du, S.-Y. Yang, Z.-S. Jin, Raman study of titania nanotube by soft chemical process, Journal of Molecular Structure. 749 (2005) 103–107. doi:10.1016/j.molstruc.2005.04.002.

[60] S.T. Nishanthi, S. Iyyapushpam, B. Sundarakannan, E. Subramanian, D. Pathinettam Padiyan, Inter-relationship between extent of anatase crystalline phase and photocatalytic activity of TiO2 nanotubes prepared by anodization and annealing method, Separation and Purification Technology. 131 (2014) 102–107. doi:10.1016/j.seppur.2014.04.047.

[61] X. Zhou, T. Shi, J. Wu, H. Zhou, (001) Facet-exposed anatase-phase TiO2 nanotube hybrid reduced graphene oxide composite: Synthesis, characterization and application in photocatalytic degradation, Applied Surface Science. 287 (2013) 359–368. doi:10.1016/j.apsusc.2013.09.156.

[62] X. Houa, J. Zhoub, S. Huanga, W. Ou-Yanga, L. Panc, X. Chena, Efficient quasi-mesoscopic perovskite solar cells using Li-doped hierarchical TiO_2 as scaffold of scattered distribution, Chemical Engineering Journal 330 (2017) 947–955. doi:10.1016/j.cej.2017.08.045.

[63] L. Tsui, T. Homma, G. Zangari, Photocurrent Conversion in Anodized TiO_2 Nanotube Arrays: Effect of the Water Content in Anodizing Solutions, The Journal of Physical Chemistry C. 117 (2013) 6979–6989. doi:10.1021/jp400318n.

[64] G.J. Brug, A.L.G. van den Eeden, M. Sluyters-Rehbach, J.H. Sluyters, The

analysis of electrode impedances complicated by the presence of a constant phase element, Journal of Electroanalytical Chemistry and Interfacial Electrochemistry. 176 (1984) 275–295. doi:10.1016/S0022-0728(84)80324-1.

[65] B. Hirschorn, M.E. Orazem, B. Tribollet, V. Vivier, I. Frateur, M. Musiani, Determination of effective capacitance and film thickness from constant-phase-element parameters, Electrochimica Acta. 55 (2010) 6218–6227. doi:10.1016/j.electacta.2009.10.065.

[66] S. Palmas, A.M. Polcaro, J.R. Ruiz, A. Da Pozzo, M. Mascia, A. Vacca, TiO2 photoanodes for electrically enhanced water splitting, International Journal of Hydrogen Energy. 35 (2010) 6561–6570. doi:10.1016/j.ijhydene.2010.04.039.

[67] P. Pu, H. Cachet, E.M.M. Sutter, Electrochemical impedance spectroscopy to study photo - induced effects on self-organized TiO2 nanotube arrays, Electrochimica Acta. 55 (2010) 5938–5946. doi:10.1016/j.electacta.2010.05.048.

[68] S. Palmas, A. Da Pozzo, M. Mascia, A. Vacca, A. Ardu, R. Matarrese, et al., Effect of the preparation conditions on the performance of TiO2 nanotube arrays obtained by electrochemical oxidation, International Journal of Hydrogen Energy. 36 (2011) 8894–8901. doi:10.1016/j.ijhydene.2011.04.105.

[69] L. Tsui, G. Zangari, Water content in the anodization electrolyte affects the electrochemical and electronic transport properties of TiO2 nanotubes: a study by electrochemical impedance spectroscopy, Electrochimica Acta. 121 (2014) 203–209. doi:10.1016/j.electacta.2013.12.163.

[70] M. Radecka, M. Rekas, A. Trenczek-Zajac, K. Zakrzewska, Importance of the band gap energy and flat band potential for application of modified TiO2 photoanodes in water photolysis, Journal of Power Sources. 181 (2008) 46–55. doi:10.1016/j.jpowsour.2007.10.082.

[71] X. Lu, G. Wang, T. Zhai, M. Yu, J. Gan, Y. Tong, et al., Hydrogenated TiO 2 Nanotube Arrays for Supercapacitors, Nano Letters. 12 (2012) 1690–1696. doi:10.1021/nl300173j.

[72] M. Radecka, M. Wierzbicka, S. Komornicki, M. Rekas, Influence of Cr on photoelectrochemical properties of TiO2 thin films, Physica B: Condensed Matter. 348 (2004) 160–168. doi:10.1016/j.physb.2003.11.086.

[73] R. van de Krol, A. Goossens, J. Schoonman, Spatial Extent of Lithium Intercalation in Anatase TiO 2, The Journal of Physical Chemistry B. 103 (1999) 7151–7159. doi:10.1021/jp9909964.

[74] Z. Wang, B. Huang, Y. Dai, X. Qin, X. Zhang, P. Wang, et al., Highly Photocatalytic ZnO / In 2 O 3 Heteronanostructures Synthesized by a Coprecipitation Method, Journal of Physical Chemistry C. 113 (2009) 4612–4617. doi:10.1021/jp8107683.

[75] Z. Jiang, X. Dai, H. Middleton, Investigation on passivity of titanium under steady-state conditions in acidic solutions, Materials Chemistry and Physics. 126 (2011) 859–865. doi:10.1016/j.matchemphys.2010.12.028.

[76] D.-S. Kong, W.-H. Lu, Y.-Y. Feng, Z.-Y. Yu, J.-X. Wu, W.-J. Fan, et al., Studying on the Point-Defect-Conductive Property of the Semiconducting Anodic Oxide Films on Titanium, Journal of The Electrochemical Society. 156 (2009) C39. doi:10.1149/1.3021008.

[77] D. Sazou, K. Saltidou, M. Pagitsas, Understanding the effect of bromides on the stability of titanium oxide films based on a point defect model, Electrochimica Acta. 76 (2012) 48–61. doi:10.1016/j.electacta.2012.04.158.

[78] B. Roh, D.D. Macdonald, Effect of oxygen vacancies in anodic titanium oxide films on the kinetics of the oxygen electrode reaction, Russian Journal of

Electrochemistry. 43 (2007) 125–135. doi:10.1134/S1023193507020012.

[79] H. Peng, First-principles study of native defects in rutile TiO2, Physics Letters A. 372 (2008) 1527–1530. doi:10.1016/j.physleta.2007.10.011.

[80] O. Carp, C.L. Huisman, A. Reller, Photoinduced reactivity of titanium dioxide, Progress in Solid State Chemistry. 32 (2004) 33–177. doi:10.1016/j.progsolidstchem.2004.08.001.

[81] U. Koning, J.W. Schultze, The examination of the influence of a space-charge layer on the formation kinetics of thin passive films by Schottky-Mott analysis, Solid State Ionics. 53-56 (1992) 255–264. doi:10.1016/0167-2738(92)90388-6.

[82] B.J. Morgan, G.W. Watson, Polaronic trapping of electrons and holes by native defects in anatase TiO2, Physical Review B. 80 (2009) 233102. doi:10.1103/PhysRevB.80.233102.

[83] H. Irie, Y. Watanabe, K. Hashimoto, Nitrogen-Concentration Dependence on Photocatalytic Activity of $TiO_{2-x}N_x$ Powders, The Journal of Physical Chemistry B. 107 (2003) 5483–5486. doi:10.1021/jp030133h.

[84] U. Kang, H. Park, Lithium ion-inserted TiO2 nanotube array photoelectrocatalysts, Applied Catalysis B: Environmental. 140 (2013) 233–240. doi:10.1016/j.apcatb.2013.04.003.

[85] B.H. Meekins, P. V Kamat, Got TiO_2 Nanotubes? Lithium Ion Intercalation Can Boost Their Photoelectrochemical Performance, ACS Nano. 3 (2009) 3437–3446. doi:10.1021/nn900897r.

[86] S.-C. Ke, T.-C. Wang, M.-S. Wong, N.O. Gopal, Low Temperature Kinetics and Energetics of the Electron and Hole Traps in Irradiated TiO_2 Nanoparticles as Revealed by EPR Spectroscopy, The Journal of Physical Chemistry B. 110 (2006) 11628–11634. doi:10.1021/jp0612578.

[87] T. Berger, M. Sterrer, O. Diwald, E. Knözinger, D. Panayotov, T.L. Thompson, et al., Light-Induced Charge Separation in Anatase TiO $_2$ Particles, The Journal of Physical Chemistry B. 109 (2005) 6061–6068. doi:10.1021/jp0404293.

[88] R. Sánchez-Tovar, R.M. Fernández-Domene, A. Martínez-Sánchez, E. Blasco-Tamarit, J. García-Antón, Synergistic effect between hydrodynamic conditions during Ti anodization and acidic treatment on the photoelectric properties of TiO2 nanotubes, Journal of Catalysis. 330 (2015) 434–441. doi:10.1016/j.jcat.2015.08.002.